
Article:
Tang, N., Zhang, B., Lord, C. orcid.org/0000-0002-2470-098X et al. (1 more author) (2020) Identification of blade operational mode shapes during wear of abradable coating. Journal of Sound and Vibration, 472. ISSN 0022-460X

https://doi.org/10.1016/j.jsv.2020.115204

Identification of blade operational mode shapes during wear of abradable coating

N. Tang[a,*], B. Zhang[a], C. Lord[a], M. Marshall[a]

[a]*Department of Mechanical Engineering, The University of Sheffield, Sheffield, S1 3JD, UK.*

Abstract

Abradable liner materials are often used in turbine engines between the compressor blade tips and the casing. The abradable liner serves as a partially sacrificial material to improve the overall engine efficiency by creating a tight seal, minimising gas flow leakage. During operation, the rubbing interaction between the blade tips and abradable lined casing induces vibrations in the blades. These vibrations not only can have a significant influence on the wear mechanism and wear efficiency of the blade tips, but also the early fatigue failure of the blades, and therefore are of interest. In this paper, a newly developed approach is presented that can be used to identify the operational blade vibration modes. A non-contact single point laser sensor is used to measure the vibrational displacements during the wear process. A mathematical transform is introduced to correct for blade position due to its rotating frame of reference. After applying the transform, the vibrational energy is calculated at various positions throughout the blade. The continuous wavelet-based modal identification is then introduced to identify the blade mode shape. The Modal Assurance Criterion (MAC) is used to demonstrate the similarity of the mode shapes as a function of wear time illustrating that the blade mode shapes change slightly with the level of wear.

Keywords: Abradable coating, vibration measurements, power spectral density, wavelet, modal identification

1. Introduction

Abradable coatings have been used in aero-engines for many years, aiming to improve the overall engine efficiency [1]. Generally, axial leakage flows influence the thermal efficiency. One of the predominate sources for this unwanted leakage is the clearance between the blade tips (compressor and turbine) and the casing, especially when wear occurs to the blade tips. A layer of the abradable coating is sprayed on the casing in order to minimise this clearance. During operation,

*Corresponding author

Email address: tang.n1988@gmail.com; n.tang@sheffield.ac.uk (N. Tang)

through local abrasion of the lining material caused by the blade tips, an effective seal is produced during operation [2].

Although the abradable coated casing can improve the engine performance, the repeated contacting between the compressor and/or turbine blades with the coating generates significant wear which induces blade vibrations [3]. As a result, the entire life of the blades can be shortened from its intended design life. Several scaled test rigs [4–7] have been developed to represent the in-service conditions for the blade tip to abradable rubbing. Wear tests using these scaled rigs have been conducted to investigate the correlations of some important factors (including abradable incursion feed rates [8, 9], contact force history [10–12], blade tip treatment [13] and abradable materials and structures [14–16]) to the wear mechanisms [17] present using in-situ measurement techniques.

Vibrations always accompany abradable coating-blade interactions, with the severity depending on the applied operational conditions. Therefore dynamics is necessary. Limited studies have considered the influences of the blade vibrations and the wear of the abradable material from the interaction with the blade. Full scaled blade tip-casing rubbing tests have been developed to show the variations of the vibrational displacements and contact force histories of the blade, when subjected to different incursion rates [9, 18]. Guo [19] observed the impact responses from the casing and identified various faults of the aero-engine using these vibrational characteristics. However, abradable samples have not been involved in the test configuration mentioned above, and this represented a simplification of the system. Fabis and Desplanques [20, 21] revealed the predominate reasons (including dynamic couplings at the blade/seal interaction, abaradable liner wear conditions and self-excited vibrations) for the amplification of the blade oscillations and quantified the vibration levels using a wavelet-based approach. However, this strategy has not been proposed to identify the vibrational shape of the blade, as only the displacement in a single location on the blade was measured in their works. Meanwhile, the contact geometry for this test rig is convex, rather than a representative concave in a real aero-engine.

Aerofoil-profile blade dynamics has been extensively studied via both numerical and experimental approaches [22–24]. The dynamic stress, especially for the 1st bending mode, has been evaluated using the strain gauges. The mode shape of the blades is then estimated using the FE and/or reduce-order method. More recently, a new test bench has been developed to evaluate the blade dynamics [25]. However, all the aforementioned researches use intrusive measurement techniques. The thermal shock may influence on the accuracy of the structural stress. To the authors' knowledges, no technique has been developed to evaluate the vibrational deflection shape of the blade directly.

In the work here, a new approach is developed to evaluate the operational mode shape of the blade. The first part of this work concentrates on the feasibility study of the application of a triangulation laser probe to monitor the displacement on the blades. The second part focuses on the post-processing algorithm developed and used to identify the operational mode shape of the blade.

2. Experimental configuration

2.1. Abradable coating rig

The test rig employed in this work was originally designed to investigate the wear mechanism between compressor/turbine blade tips and the aero-engine lining materials [4]. This test system is a representative scaled-down version that mimics the blade to abradable liner contact mechanics found in turbine engines. A flat plate with abradable material sits below a rotor that contains two opposing flat Ti-6Al-4V titanium blades. Using a linear stage, the flat plate is moved into the spinning rotor making contact with the moving blades. The rate of the incursion and the angular velocity of the rotor are controlled parameters. An image of the scaled abradable coating test rig and the drawings of the blade used are shown in Figure 1.

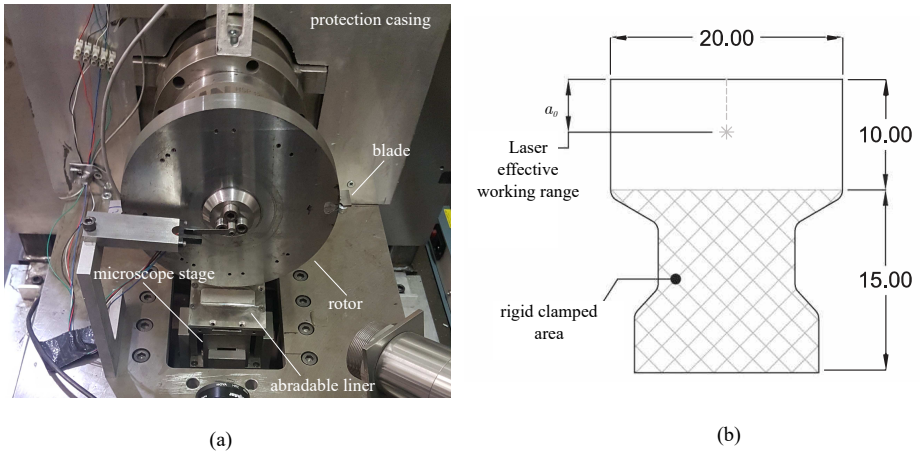

Figure 1: Overview of test setup: (a) image for the wear test rig for an abradable coating and (b) simplified blade, all units are in millimetres

Note that the measured height is defined as the distance between the top edge of the blade and the laser spot. The abradable material used in this work was plasma sprayed Metco 601NS. The material is composed of Al-7Si-40 Polyester particles originating in powder form.

The blade samples are clamped encapsulating and preloading the blades constraining the fixed end. The abradable sample is mounted on the dynamometer (Type 9347C, Kistler Instruments Ltd.) and then attached on a single axis motorised microscope stage (OSMS80-20ZF-0B, Sigma Koki Co. Ltd.). The dynamometer measures the force magnitude (both normal and tangential to the incursion), and the signals are passed into a computer via a signal conditioner (Type 5070A, Kistler Instruments Ltd.). The dynamometer is attached to a single axis motorised linear stage (OSMS80-20ZF-0B, Sigma Koki Co. Ltd.). The

motorised linear stage moves the abradable material, normal to the radial direction of the disc, into the rotating blade. The linear stage operates between 0.1 and 2000 µm s^{-1} in order to simulate the incursion feed rates from 0.02 µm/pass to 2 µm/pass. The motorised linear stage is controlled with a double channel stage controller (SHOT-202, Sigma Koki Co. Ltd.) which connects with the computer.

2.2. Selection of blade

In this work, a short 'mock' blade is used to evaluate the vibration mode shape of the blade during operation. The reason is twofold. Firstly, the mock blade can provide a relatively accurate rubbing interaction between the blade and coating material (e.g. contact force, frictional force, etc.). The excitation of the blades is determined by the interaction. Meanwhile, this interfacial contact also influences on the stiffness, and hence the dynamics of the blade. Secondly, the aim of this work is to develop a methodology to evaluate the vibration shape of blades during operation. For a real aerofoil profiled blade, both twisting and bending mode may dominate the vibration behaviour [23]. The proposed method can easily extend to identify the vibration mode for the twisting mode via adjusting the locations of the laser sensor mechanically.

The mock blade is much shorter than the real blades. The resonance frequency is much higher. The high frequency increases the difficulty in using triangulation laser to capture the vibration signal. The method can be easily applied to practical turbine blade as long as it works for the mock blade.

2.3. Optical vibration measurements

A traditional vibration measurement technique, such as the use of accelerometers, cannot be used directly on the blades in these tests due to the increase in weight to the blade and complexity due to the rotating system. The additional weight can cause variations in the blade's vibrational mode shapes and rotating imbalance. Another vibration measurement technique, that is usually used for the rotational blades, is the use of strain gauges [26]. An important issue with this technique is the operating temperature and the compatibility with the increase in heat that is generated during wear of the abradable coating. Not only is the adhesion method difficult but also the temperature compensation of the strain gauges from the thermal loads is complex and reduces the accuracy. Another issue with the use of strain gauges is the quantity required to accurately obtain high resolution mode shapes. As a result, a non-contact vibration measurement strategy is needed.

For these measurements, a full-field vibrometer would lose its effectiveness due to its low scanning speed. Therefore, a single-point laser triangulation displacement sensor (MICRO-EPSILON optoNCDT 1630-50) is used. Due to the rotating nature of the blade, the magnitude and phase can be measured along several points creating a line of measurement instead of a single point. The configuration for the laser and blade measurements are shown in Figure 2.

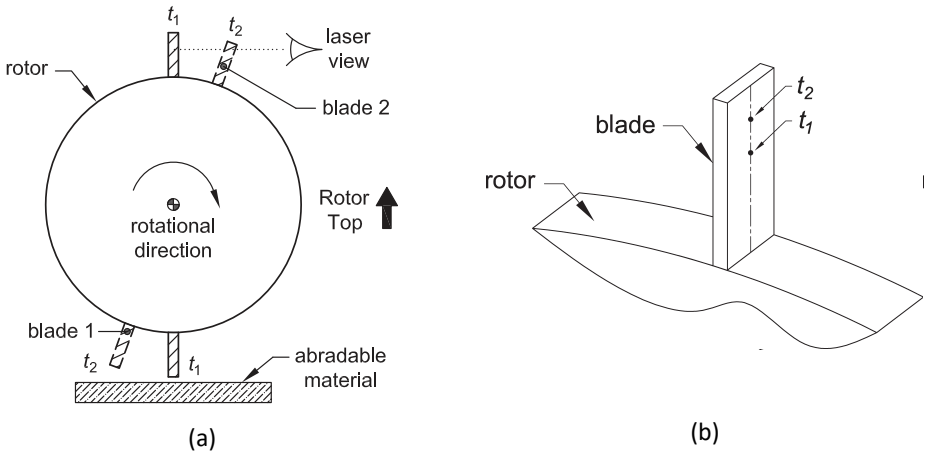

Figure 2: Schematic experiment configuration for laser measurement at time 1, t_1, and time 2, t_2, for (a) systematic diagram and (b) measurement arrangement resulting in a line measurement.

As shown in Figure 2a, the laser probe measures the blade displacements when it is rotated near the top of the rotor, while the interaction between the blade and abradable material occurs on the bottom of the rotor. The reason for this is twofold. Firstly, this configuration aims to avoid the bright sparks emitted during the wear process and the corresponding reflections. Secondly, since the blade has little damping, the response of the blade continues throughout its rotation through top dead centre. In these tests, the primary mode of interest and expected to dominate first bending mode. Therefore the laser spot is placed on the centerline of the blade, as shown in Figure 2b. For the sake of simplification of post-test signal processing, the initial measurement starts when a blade is at top/bottom dead centre. In this initial position, the distance between the lens of the laser and blade coincides with the maximum measuring range of the laser. This arrangement ensures the largest capable range of the measured height on the blade. Note that a_0 is the distance between the top most of the clamp and where the laser spot is positioned while the blade is at top dead centre.

One of the challenges in applying the laser sensor is that since the laser is stationary, the laser beam is not perfectly perpendicular to the measured surface of the blade during the rotor rotation, as illustrated in Figure 3. The main driving parameter which controls the accuracy of the laser is the location of the charge coupled device (CCD). This information is not provided by the manufacturer. This is estimated using the dimensions for the outer shell of the laser head.

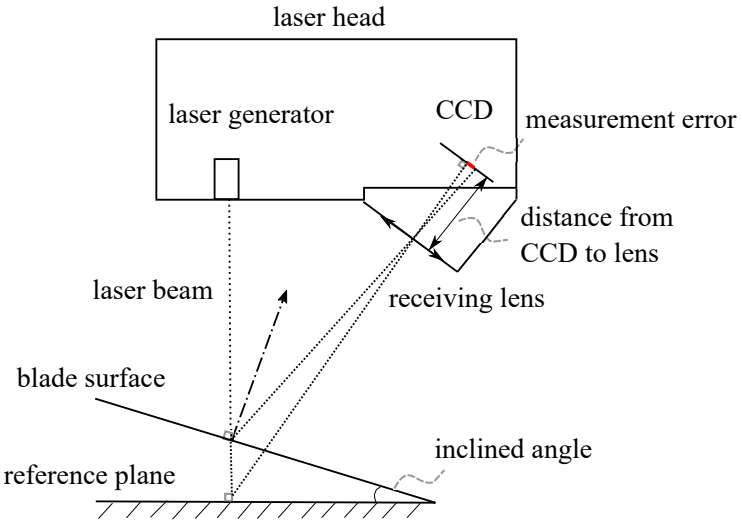

Figure 3: Schematic diagram for the errors from laser measurement

The inclined angle of the rotational blade results in the offset of the projection of the laser intensity on the CCD. This error can be evaluated using the triangulation theorem for laser measurement. Li [27] accessed the error caused by the inclined angle, and validated the developed compensation model. Using this error compensation model, the measurement errors for the current test configurations is shown in Figure 4.

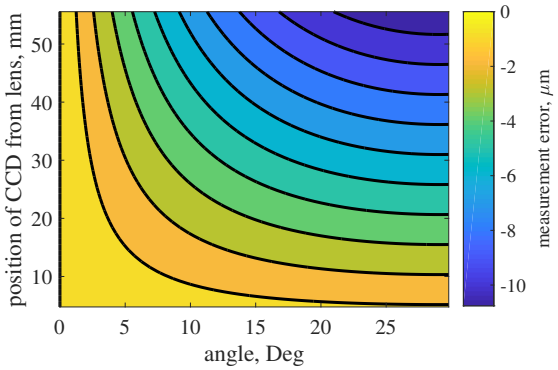

Figure 4: Errors for the laser measurement from off perpendicularity

This level of error is considered relatively small compared to the measurement range. Therefore, the inclined angle is not deemed a critical issue in the arrangement of the laser sensor.

A second issue to consider is the laser spot diameter. For this laser sensor, the spot diameter is approximately 10% of the working height of the blade.

Dorsch [28] detailed the spot intensity profile received by the CCD and hence that the identified distance profile over the spot follows a Gaussian distribution. As a result, the centre of the laser spot has the greatest influence on the distance identification. Therefore, the diameter of the laser spot is considered to have an insignificant influence on the accuracy of the measurement at a single location on the blade.

A typical collected displacement trace, over a full revolution, is shown in Figure 5.

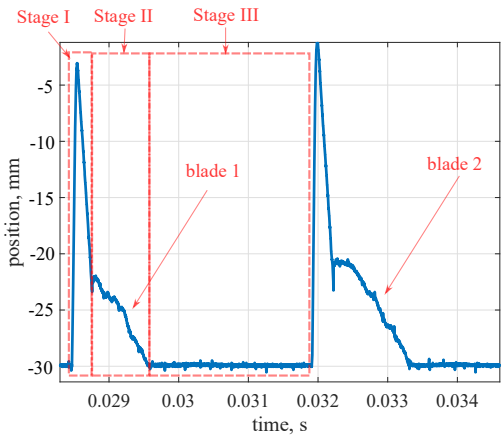

Figure 5: Typical displacement history for the collected signal

Two peaks can be observed in Figure 5 due to the existence of two nominally identical blades. Note that in Figure 5, blade 1 and blade 2 labels are not identifiers but rather just differentiators for conveyance. Physically, three different stages occur for each measured blade displacement signal. In Stage I, the laser spot hits the edge of the blade tip (while rotating upward) leading to a large sharp peak in the waveform. It is important to note that this portion of the measurement is highly inaccurate due to being an edge. The signal during Stage II has a more linear behaviour, which fits the assumption of a uniform angular velocity. The duration of this stage is defined as the useful working period of the system (or measurement range). Following this, the laser probe loses its effectiveness in Stage III, as the laser spot is no longer on the blade and the measured location is out of the useful range of the focal length for the laser probe.

3. Methodology

3.1. Noise removal algorithm

When collecting the displacement signals from the laser sensor, some noise can be observed - see Figure 5 (particularly noticeable in Stage III). As such, it is necessary to determine a method to improve the signal-to-noise ratio for the

blade displacement trace. A traditional noise removal algorithm, such as a low-pass filter or ensemble averaging is not valid in this case. When a low pass filter is introduced, the phase and shape of the waveform undergo significant change. Meanwhile, the ensemble average would eliminate the time-variant nature of the wear test, as the dynamic properties of the blade are dependent on adhesive transfer between the blade and liner during the test. Therefore, a time-domain filter, 10th order moving average filter, is introduced. The equation for this filter can be given by

$$d_{\mathrm{ma}}(t) = \frac{1}{N}\sum_{i=1}^{N} d\left[t + T_s(i-1)\right] \tag{1}$$

where N is the filter order number, i is the iteration number, t is the time and d is the original displacement signal, d_{ma} is the filtered signal and T_s is sampling period. The filtered waveform is very similar to the original one, as long as the sampling rate is high enough. In the current configuration, the sampling rate is 100 kHz. The quality and validity of this moving average filter are checked using the statistical distributions of the filtered noise, as shown in

$$\mathrm{identifiednoise} = d - d_{\mathrm{ma}} \tag{2}$$

The statistical distribution for the noise signal is illustrated in Figure 6.

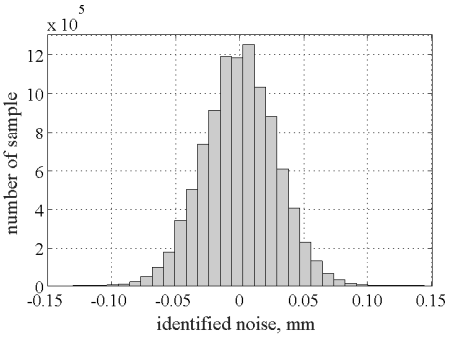

Figure 6: Statistical distribution for the error of the measurement

Figure 6 reveals a low level of identified noise, compared with the effective working range that occurs within the laser measurement (see Figure 5). Meanwhile, this noise signal follows a near normal distribution. This demonstrates that the proposed noise removal algorithm works well in the current experimental configuration.

3.2. Evaluation of the vibration energy

The power spectral density (PSD) is introduced to quantify the mean power involved for the vibration energy for each revolution.

A short-time Fourier transform (STFT) is applied to predict the vibrational 'average' power for the blade at each instantaneous time. The basis of the STFT algorithm can be seen in [29]. A brief introduction of these procedures to evaluate the vibrational energy are listed as follows:

The displacement history is separated into 10000 samples. An overlapped time between the neighbouring samples is used to ensure sufficient resolution. The frequency spectrum at a certain time is obtained using the discrete Fourier transform (DFT). This time is defined here as the mean time for each sample. When the DFT is applied to the time signal, a spectral window is also applied on each segment to avoid energy leakage. Some important parameters for the STFT in this work are listed in Table 1;

variables	value
time segment	0.1 ms
spectral window	Kaiser filter
overlap length	0.067 ms
frequency range	10-10000 Hz

Table 1: Parameters for STFT

The time-dependent PSD is then calculated using

$$P_d(\omega, t) = \frac{\left|\mathcal{F}\left[d_{\mathrm{ma}}(t)\right]\right|^2}{f_s} \tag{3}$$

where f_s is the sampling frequency, $\mathcal{F}$ is the symbol for the Fourier transform and $d_{\mathrm{ma}}(t)$ is filtered displacement signal.
Following this, the instantaneous power history is calculated using

$$P(t) = \int_{\omega_0}^{\omega_1} P_d(\omega, t) d\omega \tag{4}$$

where ω_0 and ω_1 bounds the targeted frequency ranges. In this study, only the vibrational mode of the blade is investigated. As indicated in the previous study [30], the low frequency resonances may correlate to the unbalance of the rotor shaft. This is not the interests for this study. Therefore, the lower frequency response (< 500 Hz) will not be considered here. On the other hand, the high frequency response (> 10000 Hz) will not bring significant dynamic displacements. In this work, a frequency range between 500 to 10000 Hz was selected.

Once the time-dependent power is obtained, the mean power for each revolution is calculated using the integration of the corresponding power over the corresponding time interval.

3.3. Identification of operational mode shapes

3.3.1. Kinetic analysis

Due to the measurement range limitation of the triangulation laser sensor, only a selected portion of a full revolution can be measured. In this section,

the methodology to determine this useful working time along the blade measurement range is demonstrated. The blade (along the length) measurement range is approximately 4.5mm for this configuration. This corresponds to a laser measurement range from -30 mm to -22 mm as shown in Fig 5

For the experiments presented, it is assumed that the angular velocity is constant. Under this assumption, it is further assumed that the effective working ranges for the collected signals are identical, regardless of the existence of the interaction between the blades and abradable material. Therefore, the abradable material is not involved when determining the useful working time/range.

The angular velocity is an important parameter because it links (i) the blade to the wear mechanics observed during a given point in the test and (ii) the time to the measured locations on the blade. The autocorrelation of the collected signal is introduced to estimate this rotational period. The autocorrelation of a signal [31] is defined as

$$R_{xx}(\tau) = E[d(t)\, d(t+\tau)] \tag{5}$$

where R_{xx} is the normalised autocorrelation of the displacement signal $d(t)$, and τ is the period of the signal. Physically, the autocorrelation of a signal refers to the similarity of the signal with a delayed copy of itself as a function of delay. A typical autocorrelation for the measured displacement signals is shown in Figure 7.

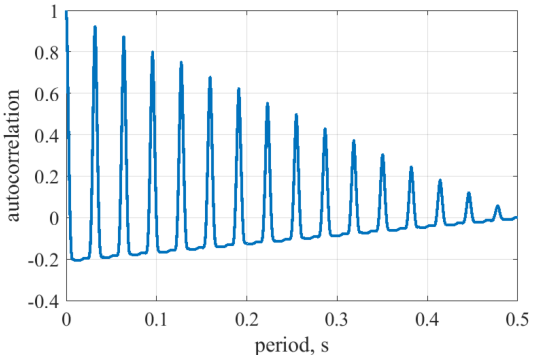

Figure 7: Typical autocorrelation for the measured signal

It can be seen from Figure 7 that several peaks occur periodically. Following this, the angular velocity can be given by

$$\omega\,(\text{inrpm}) = \frac{60}{2\tau} \tag{6}$$

where τ is the half period (as two blades' displacements are captured), identified from the second highest peak in the autocorrelation diagram (Figure 7). In this work, a half-rotational period of 0.0034 s was identified using the above mentioned method where the rotational angular velocity is approximately 8823

rpm, and the tip translational velocity is 94.7 m/s. Compared with the motor speed derived from the electrical signal input (9000 rpm), there only exists 2% difference. This indicates the accuracy of the measurement.

The effective working time of the laser is identified using the equivalence of the gradient of the displacement-time relationship between the simulated and experimental signals. For the simulated signal, it is assumed that the angular velocity is uniform and linear. A simplified sketch is illustrated in Figure 8.

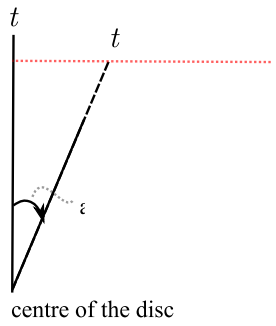

Figure 8: A schematic diagram for the laser measurement of rotational blade; the blade are rotated from time t_2 to time t_1

Using a constant uniform angular velocity, the rotational angle of the blade can be given by

$$\alpha = \frac{2\pi\omega t}{60} \tag{7}$$

The simulated displacement (b) is then expressed using the trigonometric relationship,

$$b = (a_0 + h_0)\tan\alpha \tag{8}$$

where a_0 and h_0 are defined in Figure 8. These values are defined in Section 2. A comparison between the simulated and experimental displacement history is shown in Figure 9

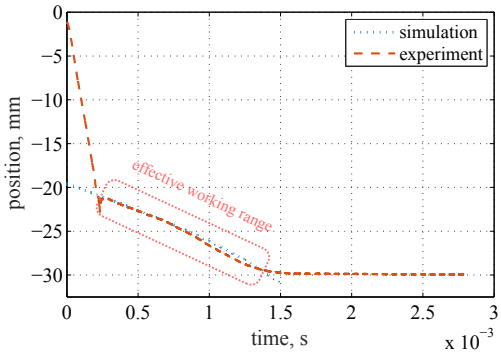

Figure 9: Identifications of the effective working range for the current laser measurement: half revolution

Figure 9 shows that the simulated displacement trace overlaps the experimental data, and the time period for the overlapped displacement is identified as the useful working time for the current measurement arrangement. Overall, the proposed method shows its effectiveness in identifying the base motion of the blade with a reasonable accuracy. Meanwhile, this figure also indicates a small difference between measured and simulated locations of the blade. This implies that the base vibration generated from the rotor is negligible small, compared with the vibration during abradable coating.

Consequently, the time-dependent measured height on the blade can be represented as,

$$h = \frac{b_{\text{measured}}}{\sin \alpha} - h_0 \tag{9}$$

3.3.2. Identification of the operational mode shape

In order to obtain the vibrational mode shape of the blade, a time-dependent modal analysis was carried out. The underlying reasons are as follows:

- The measured locations on the blade changes with time.
- The vibration of the blade changes with the progression of the wear, especially when subjected to a low incursion rate. On one hand, peak contact force is not progressive during coatings and the abradable compact can also be negligible due to the stable incursion per pass [10, 32] On the other hand, lots of adhesive interactions can be expected when subjected to a rubbing contact where release of material is poor. As it is not a clean contact, more vibration will be picked up from these interactions for a longer abradable wear track.

A wavelet-based modal analysis was selected in this work, and the detailed theoretical background can be found in [33]. The assumptions for the test configuration when applying the wavelet-based modal analysis are (i) there is low energy dissipation during each pass of the blade and (ii) each blade and

their boundary conditions are nearly identical resulting in a symmetric rotor and blades configuration.

In order to validate the first assumption, an impact hammer test is conducted to estimate the damping. At a motor frequency of 147.05Hz, a half revolution is approximately 0.00345s. Based on an estimated eigenfrequency of the blade of approximately 4000Hz and a measured damping ratio of 0.0012 (Q= 416) for the blade, holder, and disc assembly; the reduction in amplitude from the excitation is approximately 18.76% to 20.84%. This means that from the point of wear at bottom dead centre to the measurement point near top dead centre, that nearly 81.24% to 79.16% of the amplitude remains throughout the depths of incursion considered in this set of tests. Therefore, the vibrational mode shape can still be captured after the rotation of the half revolution.

During abradable coating, two different wearing mechanism, grooving or smearing of the abradable onto the blade tips and cutting wear of the tips. Based on the previous investigation [8], a net change in mass of 25 - 75 mg can be observed for the same blade and abradable material. Compared with the blade itself, the mass variation is negligible. Hence, a symmetric rotor configuration can be still assumed during abradable coating.

The oscillating displacement signal is obtained using the subtraction of free-running (no wear) signals from the one during an incursion test. The continuous wavelet transform is introduced to obtain the wavelet-based frequency response function (spectrogram) for the oscillating displacements. In this work, an analytic Morlet Wavelet is used as the mother wavelet. The magnitude in this spectrogram refers to the identified wavelet coefficient. The useful working time (measurement height a_0) and the corresponding angles of rotation are identified using the kinetic analysis. Following this, the measurement locations on the blade are correlated to the instantaneous measurement time. Since the laser beam is not perpendicular to the blade all the time, a compensation of the magnitude at different locations on the blade is used in this measurement arrangement. This equation is given by

$$\varphi_c = \frac{\varphi}{\cos\alpha} \tag{10}$$

where φ_c is the compensated magnitude, φ is the identified magnitude and α is the angle. The ratio of the peak compensated magnitude at different locations on the blade represents the operational mode shape of the blade for the selected resonance.

3.4. Validations using MAC

A comparison of mode shapes is made using the modal assurance criterion (MAC) [34]. The MAC demonstrates the similarity between the vibrational mode shapes identified for different revolutions. The MAC used in this work can be expressed as

$$\mathrm{MAC}(\varphi_i, \varphi_j) = \frac{\left|\varphi_i^T \varphi_j\right|^2}{(\varphi_i^T \varphi_j)(\varphi_j^T \varphi_i)} \tag{11}$$

	notation	unit	value
Initial measured height	a_0	mm	5.5
Radius of the rotational disc	h_0	mm	92.5
Rotor speed	ω	rpm	8823

Table 2: Key parameters of the experimental rig

where φ_i is the identified mode shape in the i^{th} revolution, φ_j is the identified mode shape in the j^{th} revolution and the superscript T refers to the Hermitian transpose. When all the elements in the MAC matrices approaches unity, these vibration modes tends to be the same validating the identification quality of this approach.

For illustration of how the mode shapes change as a function of the revolution (e.g. different amounts of wear), twelve (non-consecutive) randomly selected revolutions are used to identify the vibrational mode shapes for the same blade.

4. Results and Discussion

4.1. Measured displacement signal

This section demonstrates the typical wear debris and vibration displacement signals captured during the wear tests. In the measurements proposed here, the important operational and geometric parameters are shown in Table 2.

Following previous studies [10, 17], the incursion rate has a significant influence on the wear mechanism. For example, plucking out of complete phases from the abradable material and conventional cutting. This in turn influences high contact force that acts as the excitation of the local blade vibrations [4].

In order to examine the existence of the blade vibration, the corresponding blade and abradable samples post-tests are illustrated in Figure 10.

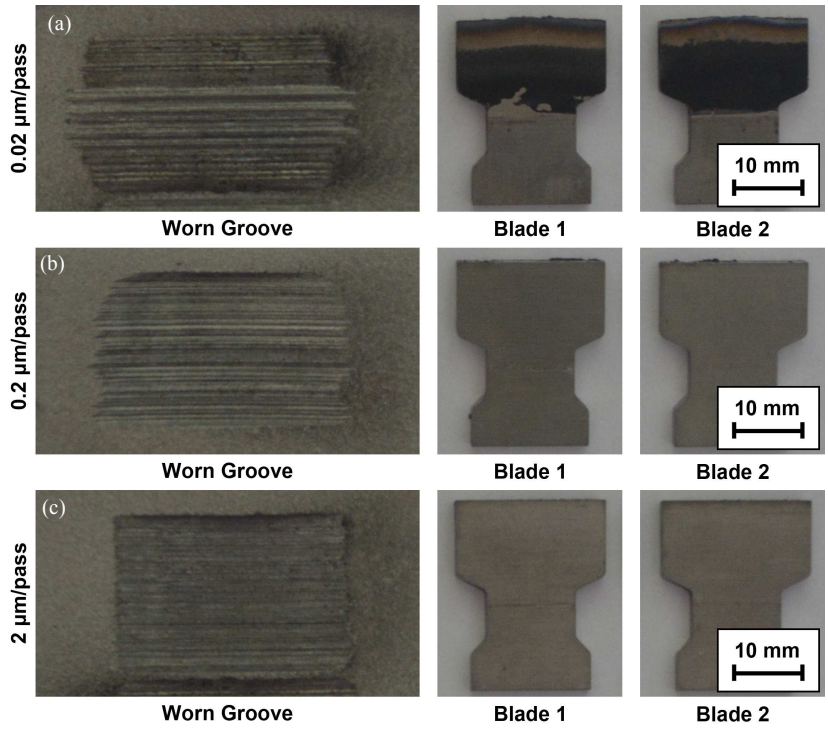

Figure 10: Blades and abradable test samples post-test for three different incursion rates; Note that 0.02 µm/pass sample were painted beforehand, in order to promote the accuracy for laser measurement

As shown in Figure 10a, at an incursion rate of 0.02 µm/pass, abradable material adheres to the blade tip. This adhesion leads to a grooved, non-uniform, wear track, and the blade now over cuts on the abradable as a consequence of the adhered material. At the intermediate incursion rate of 0.2 µm/pass (Figure 10b), adhesion to the blade is significantly reduced, leading to a more uniform and well cut wear track. However, it is apparent that some adhesion still takes place, as light grooving is still evident on the surface of the cut abradable. Finally, at the highest incursion rate of 2 µm/pass (Figure 10c), the abradable is now well cut, with adhesion to the blade negligible.

The noted change in wear mechanism with incursion rate is consistent with previous results [17] for this material, and highlights the range of interactions that occur between the blade and abradable. Of particular interest from a vibration perspective is the result at the low incursion rate, as in this case, material is adhering to the blade, and constantly changing the nature of the interaction within the system. As such, laser probe data from this test has been selected for further examination, to investigate whether this adhesion of material to the blade is accompanied by high levels of blade vibration.

In order to validate the feasibility of the developed experimental rig work during different wear test conditions, the displacement histories for the blade

subject to different incursion rates are illustrated in Figure 11.

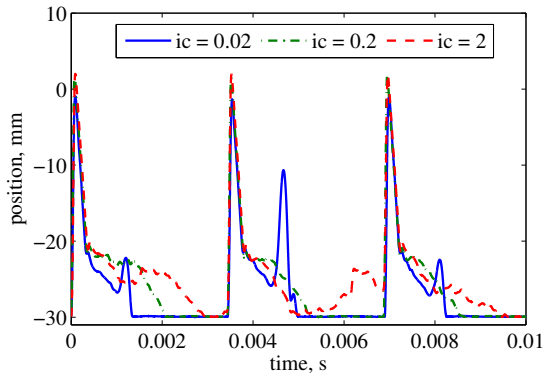

Figure 11: Typical displacement history for the abradable coatings with different incursion rates (denoted as ic with units of µm/pass)

Note that the displacement pattern only has a slight variation with time when two high incursion rates were applied. It can be seen from Figure 11 that additional peaks can always be observed in the effective working time for this wear test, and the highest peak reduces with incursion rate. This fits to the observations from Figure 10. Therefore, the developed measurement arrangement can be used to evaluate the vibrations during these tests.

4.2. Identification of the vibration energy

The typical PSD for the displacement signal is shown in Figure 12,

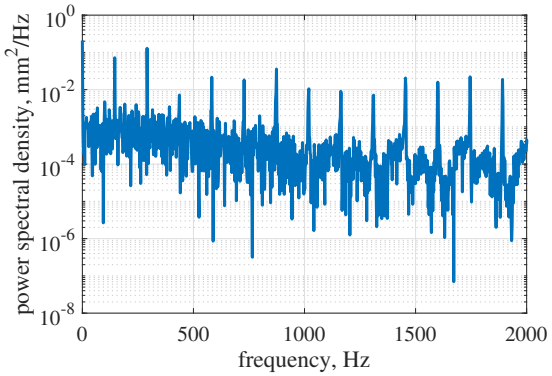

Figure 12: Typical PSD for the collected displacement signal at an incursion rate of 0.02 µm/pass

Figure 12 shows evenly spaced peaks in the frequency domain. These are indicative of the harmonics from the nonlinearity of the frictional interface in

the wear tests and play an important role in the vibration behaviour. This fits the previous findings that the predominate wear mechanism subject to low incursion rates is a rubbing/adhesive mechanism [17].

The mean power for three different incursion rates are identified and results are illustrated in Figure 13.

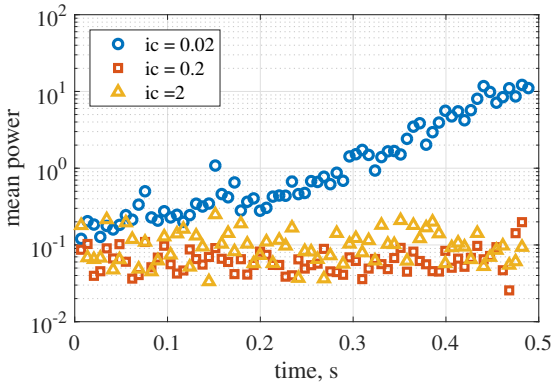

Figure 13: Mean power for each revolution subject to various incursion rates (denoted at ic with units of µm/pass)

The time-dependent mean powers have a significant difference with incursion rates. The vibrating power increases linearly when the incursion rate is 0.02 µm/pass. As noted, one of the predominate wear mechanisms is the rubbing with some abradable adhesive transfer (see Fig 10(a)). Self-excited vibrations may also be generated in this case, which leads to a more severe vibration of the blade. The wear mechanics transfers from adhesion to conventional cutting, when the incursion rate is higher than 0.06 µm/pass [10].

There is a significant increase in energy with the progression of wear when the incursion rate is 0.02 µm/pass. Less variations can be found for incursion rates of 0.2 µm/pass and 2 µm/pass. This has been witnessed in [4, 8].

4.3. Identification of blade operational mode shapes

A typical wavelet-based frequency response function for a blade subjected to a 0.02 µm/pass incursion rate test is shown in Figure 14.

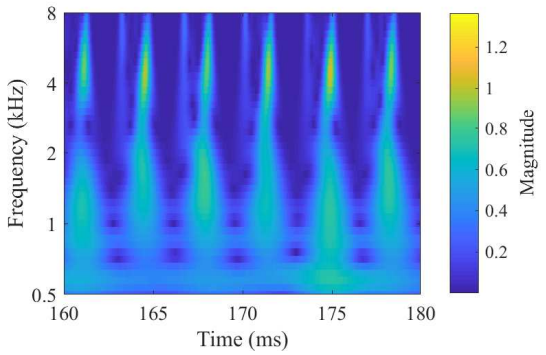

Figure 14: A typical wavelet transformed displacement signal for an incursion rate of 0.02 µm/pass

Three significant resonances can be observed in the selected frequency range between 500 and 8000 Hz. The most useful resonances for the blades can be seen in a frequency range between 3000 and 4000 Hz, based on the estimation of the resonance frequency for the same blade with a fixed boundary condition [35]. A typical displacement frequency response for different measurement times is shown in Figure 15.

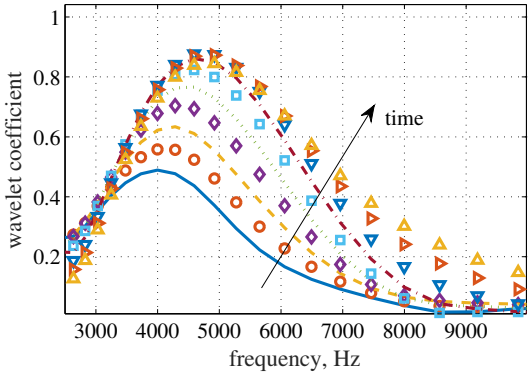

Figure 15: A typical displacement frequency response for different times in a given revolution for an incursion rate of 0.02 µm/pass

Figure 15 shows a typical wavelet coefficient-frequency relationship. The peak shifts towards higher frequencies with the increments of the measured locations. This variation is thought to be related to the excitation forces. When the blade is rubbing the abradable liner, the maximum contact force is applied on the blade and hence causes the greatest frictional force. The frictional force involved in the system drops with further rotation in the same revolution. With the decrease of frictional force, the resonant frequency increases. The identified

vibrational mode shape is illustrated in Figure 16.

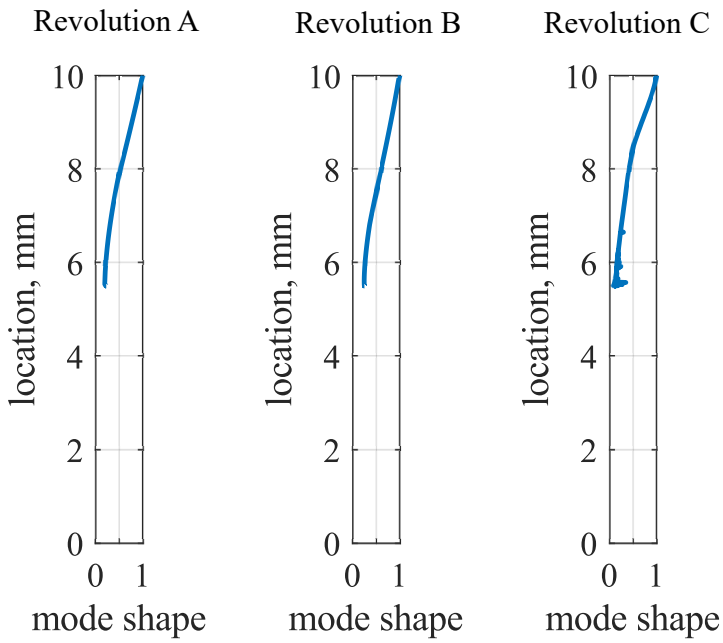

Figure 16: Typical mode shapes identified at three different randomly selected revolutions for an incursion rate of 0.02 µm/pass where Revolution A occurs before Revolution B which occurs before Revolution C

It can be seen from Figure 16 that all of the three identified vibrational mode shapes follows the typical fundamental bending mode for a flat uniform cross-secion with fixed-free boundary conditions. Approximately 50% of the unconstrained height of the blade can be measured using the proposed measurement arrangement in these experiments. The mode shape over the whole range of the height could be captured, when a proper initial height is selected.

To show how the mode shapes change with wear progression, the modal assurance criteria (MAC) of the mode shapes identified from 12 randomly selected revolutions are shown in Figure 17.

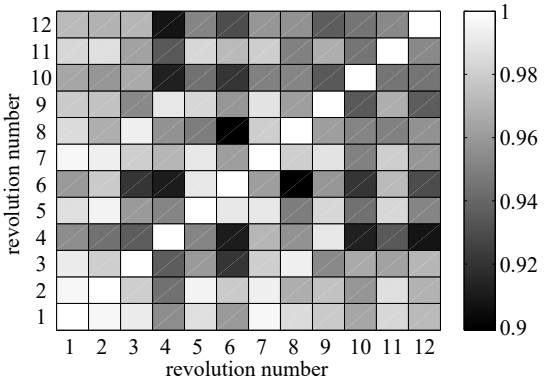

Figure 17: MAC for the mode shapes identified from 12 randomly selected revolutions

The MAC is a statistical tool to compare the degree of consistency between the mode shapes. This statistic indicator is most sensitive to large differences in the mode shapes. Showing that the diagonal elements are nearly unity leads to demonstration that each selected revolution is unique. Further to this, the off diagonal magnitudes are off unity further validating that each mode is independent in shape to the other mode shapes.

5. Conclusions

This paper develops a novel procedure to monitor the vibration mode during the abradable wear process using a non-contact technique. This configuration has been shown its capability to evaluate both vibrational energy and then determine mode shape of the blade. This developed technique demonstrates that with a non-contact single point laser sensor, several points can be measured from a single measurement. This provides a clear benefit where the captured mode shape has a high spatial resolution which is significantly larger than what could be achieved with the implementation of either accelerometers or strain gauges. The power spectral density is introduced, in order to represent the vibrational (strain) energy for the blade. This method is discussed through the study on the influence of the incursion rates. It is shown that a low incursion rate results in a relatively high magnitude of vibration energy and that the vibration energy tends to be consistent during operation when the incursion rate exceeds to a certain level. This observation is consistent with the previous study [4], and therefore shows the feasibility of the proposed method. The wavelet-based modal analysis has been applied to monitor the vibrational mode shapes of the blades during this wear test. Using the modal assurance criterion, it has been shown that the mode shapes change slightly as a function of the revolution (amount of wear). This proposed method demonstrates the benefits not only for its non-contact capabilities and high resolution and accuracy, but also for the fast acqusition of the mode shapes illustrating the novelty of the approach.

Conflict of interest

The authors declare that they have no conflict of interest.

References

[1] D. Sporer, A. Refke, M. Dratwinski, M. Dorfman, S. Metco, I. Giovannetti, M. Giannozzi, M. Bigi, New high-temperature seal system for increased efficiency of gas turbines, Sealing technology 2008 (2008) 9–11.

[2] W. Dalzell Jr, S. Sanders, G. Crawford, F. Walden, W. Woodard, Abradable seal having improved properties, 2002. US Patent 6,352,264.

[3] A. Millecamps, J. Brunel, P. Dufrénoy, F. Garcin, M. Nucci, Influence of thermal effects during blade-casing contact experiments, in: ASME 2009 International Design Engineering Technical Conferences and Computers and Information in Engineering Conference, American Society of Mechanical Engineers, 2009, pp. 855–862.

[4] J. Stringer, M. Marshall, High speed wear testing of an abradable coating, Wear 294 (2012) 257–263.

[5] G. Sutter, S. Philippon, F. Garcin, Dynamic analysis of the interaction between an abradable material and a titanium alloy, Wear 261 (2006) 686–692.

[6] C. Padova, J. Barton, M. Dunn, S. Manwaring, G. Young, M. Adams, M. Adams, Development of an experimental capability to produce controlled blade tip shroud rubs at engine speed, Journal of turbomachinery 127 (2005) 726–735.

[7] C. Padova, M. Dunn, J. Barton, K. Turner, T. Steen, Controlled fan blade tip/shroud rubs at engine conditions, in: ASME 2011 Turbo Expo: Turbine Technical Conference and Exposition, American Society of Mechanical Engineers, 2011, pp. 951–961.

[8] N. Fois, J. Stringer, M. Marshall, Adhesive transfer in aero-engine abradable linings contact, Wear 304 (2013) 202–210.

[9] C. Padova, J. Barton, M. Dunn, S. Manwaring, Experimental results from controlled blade tip/shroud rubs at engine speed, Journal of Turbomachinery 129 (2007) 713–723.

[10] N. Fois, M. Watson, J. Stringer, M. Marshall, An investigation of the relationship between wear and contact force for abradable materials, Proceedings of the Institution of Mechanical Engineers, Part J: Journal of Engineering Tribology 229 (2015) 136–150.

[11] B. Wang, J. Zheng, G. Lu, Rubbing contact between rotating blade and casing plate, Part 1–Experimental study, in: Key Engineering Materials, volume 233, Trans Tech Publ, 2003, pp. 725–730.

[12] J. Vincent, S. Philippon, A. Cappella, J. Meriaux, S. Selezneff, Enhancement of an experimental method to measure accurately the evolution of forces during short-lived interactions: Application to blade-abradable material contacts in turbomachines, Measurement 98 (2017) 167–178.

[13] M. Watson, N. Fois, M. Marshall, Effects of blade surface treatments in tip–shroud abradable contacts, Wear 338 (2015) 268–281.

[14] B. Zhang, M. Marshall, Investigating the application of a honeycomb abradable lining in the turbine stage of an aero-engine, Tribology International 125 (2018) 66–74.

[15] W. Xue, S. Gao, D. Duan, Y. Liu, S. Li, Material transfer behaviour between a ti6al4v blade and an aluminium hexagonal boron nitride abradable coating during high-speed rubbing, Wear 322 (2015) 76–90.

[16] E. Irissou, A. Dadouche, R. Lima, Tribological characterization of plasma-sprayed CoNiCrALY-BN abradable coatings, Journal of Thermal Spray Technology 23 (2014) 252–261.

[17] M. Watson, M. Marshall, Wear mechanisms at the blade tip seal interface, Wear 404 (2018) 176–193.

[18] N. Langenbrunner, M. Weaver, M. Dunn, C. Padova, J. Barton, Dynamic response of a metal and a cmc turbine blade during a controlled rub event using a segmented shroud, Journal of Engineering for Gas Turbines and Power 137 (2015) 062504.

[19] C. Guo, Study on the recognition of aero-engine blade-casing rubbing fault based on the casing vibration acceleration, Measurement 65 (2015) 71–80.

[20] S. Baïz, J. Fabis, X. Boidin, Y. Desplanques, Experimental investigation of the blade/seal interaction, Proceedings of the Institution of Mechanical Engineers, Part J: Journal of Engineering Tribology 227 (2013) 980–995.

[21] R. Mandard, J. Witz, Y. Desplanques, J. Fabis, J. Meriaux, Wavelet analysis of experimental blade vibrations during interaction with an abradable coating, Journal of Tribology 136 (2014) 031102.

[22] A. Batailly, M. Legrand, A. Millecamps, F. Garcin, Numerical-experimental comparison in the simulation of rotor/stator interaction through blade-tip/abradable coating contact, Journal of Engineering for Gas Turbines and Power 134 (2012) 082504.

[23] A. Batailly, Q. Agrapart, A. Millecamps, J. Brunel, Experimental and numerical simulation of a rotor/stator interaction event localized on a single blade within an industrial high-pressure compressor, Journal of Sound and Vibration 375 (2016) 308–331.

[24] M. Antoine, Interaction aube-carter: contribution de l'usure de l'abradable et de la thermomcanique sur la dynamique d'aube, Ph.D. thesis, University of Lille, 2010.

[25] S. Nitschke, T. Wollmann, C. Ebert, T. Behnisch, A. Langkamp, T. Lang, E. Johann, M. Gude, An advanced experimental method and test rig concept for investigating the dynamic blade-tip/casing interactions under engine-like mechanical conditions, Wear 422 (2019) 161–166.

[26] P. Russhard, The rise and fall of the rotor blade strain gauge, in: Vibration Engineering and Technology of Machinery, Springer, 2015, pp. 27–37.

[27] B. Li, F. Li, H. Liu, H. Cai, X. Mao, F. Peng, A measurement strategy and an error-compensation model for the on-machine laser measurement of large-scale free-form surfaces, Measurement Science and Technology 25 (2013) 015204.

[28] R. Dorsch, G. Häusler, J. Herrmann, Laser triangulation: fundamental uncertainty in distance measurement, Applied optics 33 (1994) 1306–1314.

[29] P. Welch, The use of fast fourier transform for the estimation of power spectra: a method based on time averaging over short, modified periodograms, IEEE Transactions on audio and electroacoustics 15 (1967) 70–73.

[30] J. Hong, T. Li, Z. Liang, D. Zhang, Y. Ma, Research on blade-casing rub-impact mechanism by experiment and simulation in aeroengines, Shock and Vibration 2019 (2019).

[31] D. Newland, An introduction to random vibrations, spectral & wavelet analysis, Courier Corporation, 2012.

[32] N. Zhang, J. Shen, H. Xuan, Y. Hu, W. Hong, Evaluation of an Alsi-polyester abradable seal coating performance using high-temperature and high-velocity abrasion tests, Proceedings of the Institution of Mechanical Engineers, Part J: Journal of Engineering Tribology 230 (2016) 842–851.

[33] T. Le, P. Argoul, Continuous wavelet transform for modal identification using free decay response, Journal of Sound and Vibration 277 (2004) 73–100.

[34] R. Allemang, D. Brown, A correlation coefficient for modal vector analysis, in: Proceedings of the 1st international modal analysis conference, volume 1, SEM Orlando, 1982, pp. 110–116.

[35] R. Blevins, R. Plunkett, Formulas for natural frequency and mode shape, Journal of Applied Mechanics 47 (1980) 461.